PROCEEDINGS OF SPIE

SPIEDigitalLibrary.org/conference-proceedings-of-spie

A 3D imaging system integrating photoacoustic and fluorescence orthogonal projections for anatomical, functional and molecular assessment of rodent models

Hans P. Brecht, Vassili Ivanov, Diego S. Dumani, Stanislav Y. Emelianov, Mark A. Anastasio, et al.

Hans P. Brecht, Vassili Ivanov, Diego S. Dumani, Stanislav Y. Emelianov, Mark A. Anastasio, Sergey A. Ermilov, "A 3D imaging system integrating photoacoustic and fluorescence orthogonal projections for anatomical, functional and molecular assessment of rodent models," Proc. SPIE 10494, Photons Plus Ultrasound: Imaging and Sensing 2018, 1049411 (16 March 2018); doi: 10.1117/12.2290880

SPIE.

Event: SPIE BiOS, 2018, San Francisco, California, United States

A 3D imaging system integrating photoacoustic and fluorescence orthogonal projections for anatomical, functional and molecular assessment of rodent models

Hans P. Brecht[1], Vassili Ivanov[1], Diego S. Dumani[2,3], Stanislav Y. Emelianov[2,3], Mark A. Anastasio[4], Sergey A. Ermilov[1]

[1]PhotoSound Technologies, Inc., 5658 Sylmar Rd., Houston, Texas 77081, USA

[2]Wallace H. Coulter Dept. of Biomedical Engineering, Georgia Institute of Technology and Emory University School of Medicine, 777 Atlantic Dr., Atlanta, Georgia 30332, USA

[3]School of Electrical and Computer Engineering, Georgia Institute of Technology, 777 Atlantic Dr., Atlanta, Georgia 30332, USA

[4]Dept. of Biomedical Engineering, Washington University in St. Louis, One Brookings Dr., St. Louis, Missouri 63130, USA

ABSTRACT

We have developed a preclinical 3D imaging instrument integrating photoacoustic tomography and fluorescence (PAFT) addressing known deficiencies in sensitivity and spatial resolution of the individual imaging components. PAFT is designed for simultaneous acquisition of photoacoustic and fluorescence orthogonal projections at each rotational position of a biological object, enabling direct registration of the two imaging modalities. Orthogonal photoacoustic projections are utilized to reconstruct large (21 cm^3) volumes showing vascularized anatomical structures and regions of induced optical contrast with spatial resolution exceeding 100 µm. The major advantage of orthogonal fluorescence projections is significant reduction of background noise associated with transmitted or backscattered photons. The fluorescence imaging component of PAFT is used to boost detection sensitivity by providing low-resolution spatial constraint for the fluorescent biomarkers. PAFT performance characteristics were assessed by imaging optical and fluorescent contrast agents in tissue mimicking phantoms and in vivo. The proposed PAFT technology will enable functional and molecular volumetric imaging using fluorescent biomarkers, nanoparticles, and other photosensitive constructs mapped with high fidelity over robust anatomical structures, such as skin, central and peripheral vasculature, and internal organs.

Keywords: Photoacoustic tomography, optical imaging, preclinical imaging, molecular imaging, small animal models, cancer imaging, quantitative imaging

1. INTRODUCTION

Optical *in vivo* imaging methods allow affordable, convenient, and highly sensitive interrogation of molecular microenvironments and physiological processes in biomedical rodent models.[1-5] Modern fluorescence methodologies achieve high sensitivity in whole body mouse imaging using far red or near infrared (NIR) genetically encoded markers or dyes.[6,7] However, commercial optical imaging systems for *in vivo* research suffer from poor spatial resolution.

Three-dimensional photoacoustic tomographic (PAT) imaging previously demonstrated 150-500 µm resolution in high-fidelity 3D whole body mice images.[8-11] Hemoglobin, the dominant endogenous chromophore in the near infrared optical range, is responsible for superior optical contrast of blood-rich tissues.[12] Accordingly, PAT of live mice can provide high fidelity 3D anatomical maps of skin, vascular tree, and blood rich organs (kidney, spleen, liver, intestine, and heart) with less than 1 minute scans. Abundant anatomical and physiological information available via PAT images helps scientists to

Photons Plus Ultrasound: Imaging and Sensing 2018, edited by Alexander A. Oraevsky, Lihong V. Wang, Proc. of SPIE Vol. 10494, 1049411 · © 2018 SPIE · CCC code: 1605-7422/18/$18 · doi: 10.1117/12.2290880

study various pathological conditions, including cancer, trauma, ischemia, and stroke.[13] PAT was also successfully used for preclinical assessment of thermal therapies and biodistribution of optical contrast agents and fluorescent proteins.[14-20] A few clinical applications of 3D PAT including peripheral angiography and diagnostics of breast cancer are being investigated.[21,22] PAT is also attractive from a perspective of molecular imaging, since it can use the same instrumentation for excitation of fluorescence and generation of photoacoustic effect.[23-25] However, due to a strong background signal generated by native blood, its sensitivity to detection of fluorophores is inferior with respect to conventional fluorescence techniques.[26,27]

In this report we describe a new pre-clinical 3D imaging modality, which integrates photoacoustic and fluorescence detection channels (PAFT) in a compact table-top design. PAFT is designed to enable unparallel combination of functional and molecular sensitivity, spatial resolution, and localization of fluorescently labeled biological structures and processes mapped with high fidelity over robust anatomical structures, such as skin, central and peripheral vasculature, and internal organs. Such prominent biomedical research areas as cancer, toxicology, tissue engineering and regeneration, cardiovascular and developmental biology would greatly benefit from the PAFT technology providing in vivo tracking, mapping, and longitudinal studies of externally labeled or internally expressed light-emitting or absorbing molecular constructs.

2. SYSTEM DESIGN

PAFT concept was implemented via co-registered integration of fluorescence and photoacoustic modalities in a single compact 3D configuration defeating shortcomings of each individual technology. The design features orthogonal orientation of both imaging channels: optical and photoacoustic. It means that the direction of optical excitation light is perpendicular to the direction of both photoacoustic and optical detection. The orthogonal photoacoustic excitation reduces high-amplitude imaging clutter produced by light absorbed in skin and bulk tissue. The orthogonal excitation of fluorescence reduces background noise from transmitted of scattered photons. The excitation of photoacoustic waves and fluorescence occurs simultaneously enabling co-registration of the two images.

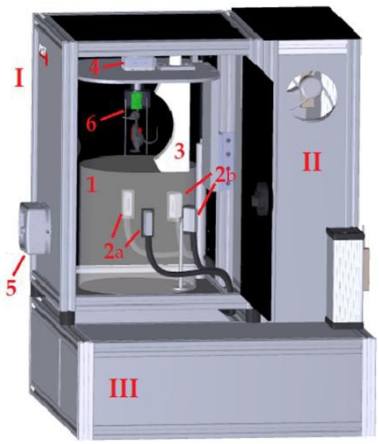

The developed prototype of the PAFT instrument (Figure 1) had a footprint of 21.5" x 21.5" and height of 26.5", occupying just 1/3 of a small lab bench. The chassis was designed to incorporate an imaging module (I), closed loop water circulation, heating and degassing system, data acquisition unit, and control unit. The electronics (II) was fully separated from the imaging module and the wet compartment (III) at the bottom, minimizing moisture and risk of accidental flood.

Figure 1: Parts and components of the PAFT prototype. (I) imaging module, (II) dry electronics compartment, (III) wet compartment. Imaging module consists of: (1) water tank; (2) fiberoptic illuminators (a – orthogonal excitation, b – epi-illumination); (3) photoacoustic array detector; (4) rotary stage; (5) optical detection unit; (6) animal restrainer & anesthesia delivery unit.

PAFT employs a 3D rotational tomographic configuration for both photoacoustic and fluorescence imaging channels. The imaging module (I) is the key unique component enabling functionality of the PAFT system. It consists of the transparent acrylic water tank filled with coupling medium (1), fiberoptic laser excitation termini (2a – orthogonal, 2b – epi-illumination), photoacoustic array probe (3), rotary stage (4), optical camera detector (5) with optical filters optimized for the fluorescence emission wavelength, and the animal restrainer and anesthesia delivery unit (6).

A pulsed optical parametric oscillator (OPO) system (Phocus HE Mobile, Opotek, Carlsbad, CA) allowing wide range of near infrared (NIR) tunable output is used for orthogonal excitation of fluorescence and photoacoustic waves. The OPO laser source runs at 10 Hz frame rate producing 6-ns pulses of 130 mJ peak energy. The OPO output can be tuned in the range 690-950 nm and 1200-2400 nm. A separate laser output emits the second harmonic (λ = 532 nm) of the Nd:YAG OPO pump laser. It is attenuated to 2 mJ per pulse, and it is reserved for future anatomical photoacoustic imaging of skin and superficial blood vessels. The laser excitation light is delivered to the imaging tank via two separate randomized 1 in

– 2 out fiberoptic bundles. Each fiberoptic output is split into two individual rectangular apertures (2 mm x 20 mm), providing 25 mm tall bi-lateral illumination pattern on the surface of the interrogated object.

The PAFT prototype contained a water-proof photoacoustic detector array (PhotoSound Technologies, Houston, TX) of 96 piezo-composite omnidirectional ultrasonic transducers arranged over a vertical arc of 118°. All the transducers in such a geometry are directed towards the center of reconstructed volume, minimizing negative effects of the finite transducer's directivity on the quality of reconstructed optoacoustic images. The detector radius of 65 mm enabled loading of the animal from the top of the imaging module. Each transducer element had a 1.3 mm x 1.3 mm rectangular shape, 6 MHz center frequency and 60% acoustic bandwidth (-6 dB, transmit/receive mode). The probe was fixed on the lid of the imaging module to maintain consistent tomographic geometry and reduce risk of misalignment during cleaning and maintenance.

A compact (165 mm x 165 mm x 56 mm) photoacoustic data acquisition unit (DAQ) was developed and manufactured by PhotoSound Technologies (Houston, TX). The 96-channel DAQ is built on 16-ch variable gain amplifier (VGA) with octal high-speed ADC microchip AFE5851 by Texas Instruments (Austin, TX). The total desired gain (up to 64 dB) is established by a built-in amplifier with gain programmable between -5 and 31 dB and an additional preamplifier circuit (33 dB, 0.1 – 10 MHz bandwidth at -6 dB) accommodating electrical properties of the photoacoustic detector probe. Photoacoustic data is sampled in parallel on all 96 channels at 12-bit resolution, 2.5-32.5 MHz sampling rate, and 4096 samples per channel, allowing photoacoustic interrogation of biological tissue with maximum resolution at up to 190 mm away from the probe. The acquisition of photoacoustic data is typically triggered by an external TTL signal (laser Q-switch emission output) or directly by a laser pulse using an embedded photodiode trigger circuit at frame rates up to 20 Hz. A programmable trigger delay is also available. The DAQ unit communicates with a Windows PC computer via a USB 2.0 interface. The board is safely powered by 12V and <2.5A DC. The DAQ PC drivers were embedded in the LabView scanning environment, enabling 3D PAT and fluorescence data acquisition procedures. A graphical user interface (GUI) allowed setup, initiation and storage of the scan data. A separate Matlab imaging software was developed allowing reconstruction of single-wavelength PAT volumes. Digital signal conditioning included the running average adjusted according to the voxel size and the 12^{th} order low-pass zero-phase Butterworth filter with a cut-off frequency of 8 MHz (-3 dB). Standard filtered backprojection (FBP) algorithm[28-30] was used for PAT.

The PAFT prototype was designed for rotational tomographic scanning of live anesthetized mice. Each 360° imaging scan was performed by a piezo rotary stage with the azimuthal position encoder PR-50-11200 (Micronix, Irvine CA), programmed to move in continuous mode. The mouse restrainer was designed to operate with a standard free-breathing anesthesia delivery system. The principle of operation of the underwater mouse breathing system resembles a "diving bell" and was described in the previous publications.[8,9,15] The water temperature inside the imaging tank was maintained at 37 ± 0.5 °C by a temperature control system using embedded thermocouples and heating elements. Closed loop circulation was implemented to improve thermal and acoustic homogeneity of the heated water. The latter was established by in-line degassing unit.

A scientific 16-bit 4MP CMOS camera Dhyana 400D (Tucsen Photonics, China) was installed in the imaging module opposite to and directly facing the photoacoustic probe (Figure 1). The camera was equipped with an imaging objective providing 50 mm x 50 mm images of the studied object and the fluorescence emission filter matching the emission spectrum of the studied fluorophore (in these studies – indocyanine green or ICG). The inside of the imaging module and all the components illuminated during a scan were black coated to reduce background fluorescence. The camera shutter was triggered to open for 20 ms on each laser pulse with a delay of 90 ms to ensure maximum exposure for the following laser pulse. The camera recorded a video of the entire scan or a set of *.tiff images showing multiple radial views of the interrogated object.

3. IMAGING PERFORMANCE

Two types of optically transparent phantoms were developed and fabricated to evaluate the limits of resolution and sensitivity of PAFT imaging in the photoacoustic mode. The resolution phantom consisted of two ∅150 μm plastic optically absorbing microfilaments (PowerPro, Irvine, CA). The microfilaments were set intersecting in an X-shaped pattern elongated along the z-axis of rotation within the PAFT imaging module. Only the transverse (xy) resolution could be evaluated using this type of phantom. Figure 2a shows the 3D PAT image of the resolution phantom represented by multiple radial views imitating its rotation during the PA scan. High contrast and few imaging artifacts are evident. The xy resolution was estimated from the scaled 10mm x10mm crossectional images of the phantom (Figure 2b). For each xy

section, the diameter of each microfilament image was measured in x and y directions, then averaged for all 4 measurements. The xy resolution was estimated to be between 45 µm and 117 µm by subtracting the actual diameter of the microfilament (150 µm) from the diameter estimated from a crossectional image. Significant systematic change of the transverse resolution along z-axis indicates either a radial offset of the PA probe (image reconstruction algorithm requires a spherical detection configuration with r = 65 mm) or a possible ±2 mm deviation of the PA probe's radius dictated by the manufacturing tolerances.

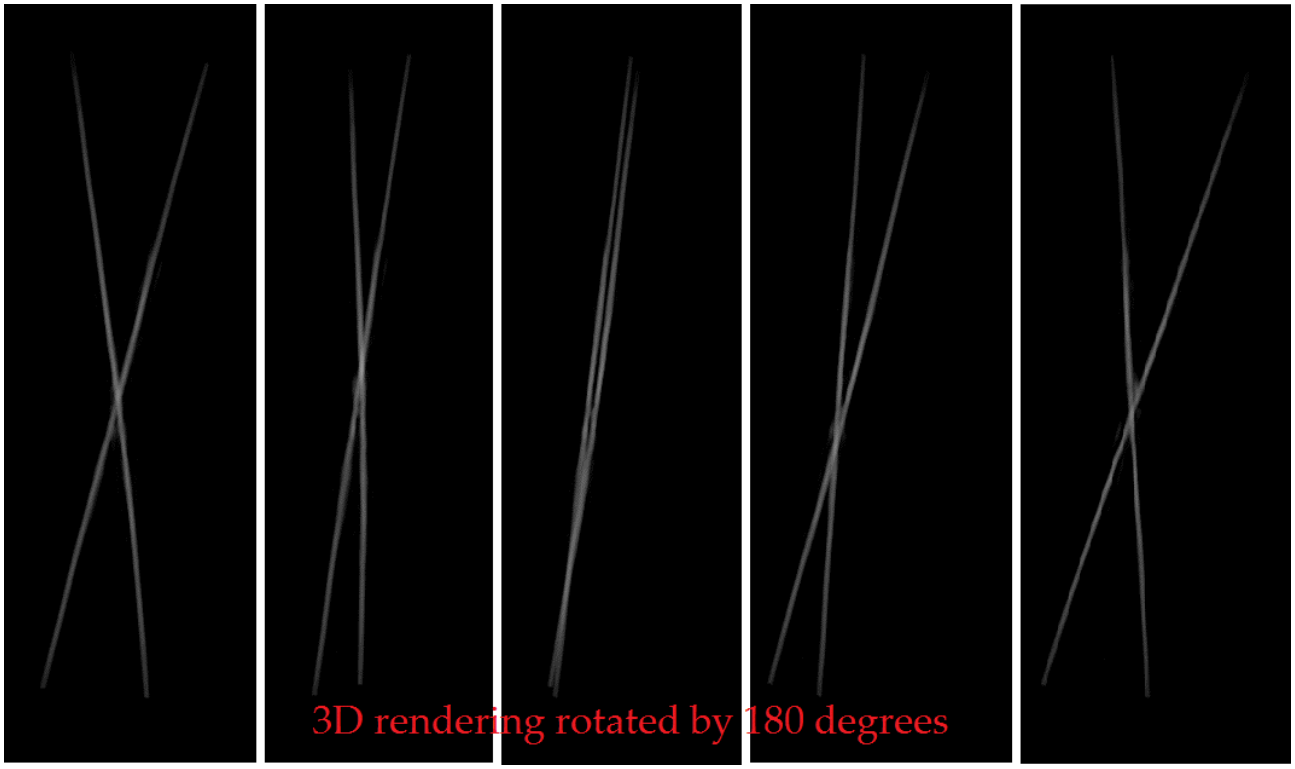

(a)

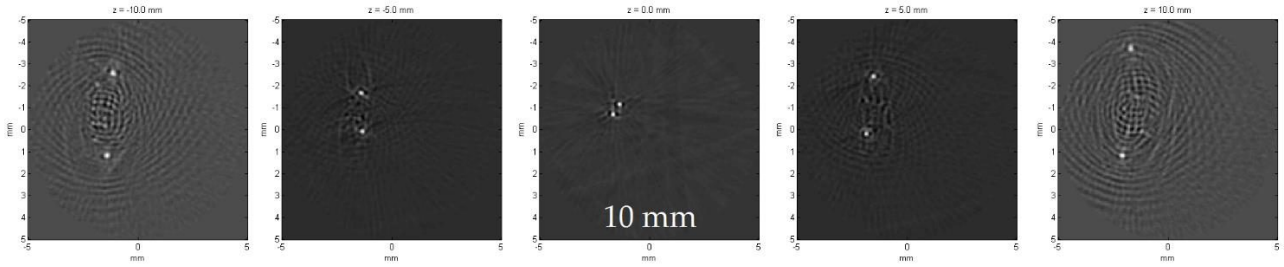

(b)

Figure 2: (a) Three-dimensional PAT image of the X-shaped resolution phantom; each panel is rotated by 45°. (b) 10 mm x 10 mm horizontal (xy) crossections of the 3D PAT image of the resolution phantom at (left to right) z = -10 mm, -5 mm, 0 mm, 5 mm, and 10 mm.

The sensitivity phantom consisted of six vertically oriented ultrathin PTFE tubes (0.635 mm ID and 0.05 mm wall thickness) filled with samples of $CuSO_4$ solution. The stock sample had optical density OD = 2 cm^{-1} at the excitation wavelength of 800 nm. Four other tubes contained $CuSO_4$ samples created by dilution of the stock solution to 1/2, 1/4, 1/8, and 1/16. A control sample of DI water was inserted between the stock and 1/2 samples. The output OPO energy was 20 mJ/pulse. The used fiberoptic light delivery bundles had optical transmission of T = 50%. Figure 3 shows a single 30 mm

x 30 mm horizontal (xy) crossection of the reconstructed PAT volume of the sensitivity phantom. Four out of five sample tubes are clearly visible over the background with contrast increasing according to the increase in optical absorption of the samples. The control DI water tube is not visible (its location is labeled "W" in the Figure 3), demonstrating that the Teflon material of the tubes did not produce measurable photoacoustic response. The sample with the lowest absorption coefficient, which is still visible is labeled "1/8", μ_{amin} = 0.57 cm^{-1} (1/8 OD2). We estimate that the PA sensitivity of the PAFT instrument can be improved 11x by using the maximum energy of the Phocus HE Mobile OPO (120 mJ/pulse), and higher transmission fiberoptic excitation bundles (T = 90%), providing minimum detectable optical absorption coefficient of μ_{amin} = 0.05 cm^{-1} for a ∅0.635 mm cylindrical object, like a medium-sized blood vessel.

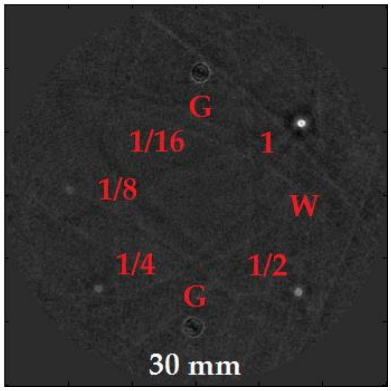

Figure 3: A 30 mm x 30 mm horizontal (xy) crossection of the 3D PAT image of the sensitivity phantom at z = 0 mm. Samples of $CuSO_4$ solution are numbered according to their respective optical densities (OD) at 800 nm excitation laser wavelength. W – control sample with DI water. G – garolite phantom support rods.

4. IN VIVO IMAGING

The pilot in vivo study was focused on initial testing and characterization of the PAFT-3D imaging system using normal mice. BALB/c female nu/nu mice (Charles River Laboratories), 5-6 weeks of age were used under the procedures of the IACUC protocol approved at the Georgia Institute of Technology. For PAFT imaging, the sedated mouse's head was placed within a breathing cone, to allow anesthesia to be freely administered, and positioned into a restraining frame for imaging. The temperature inside the immersion water bath was maintained at 37 ± 0.1 °C. The animal was submerged up to the chin, in a neutral buoyancy upward position. Each PAFT scan lasted about 30 seconds. Laser excitation wavelength was tuned to 760 nm. Optical fluence at the skin level of the mouse was 1.8 mJ/cm^2.

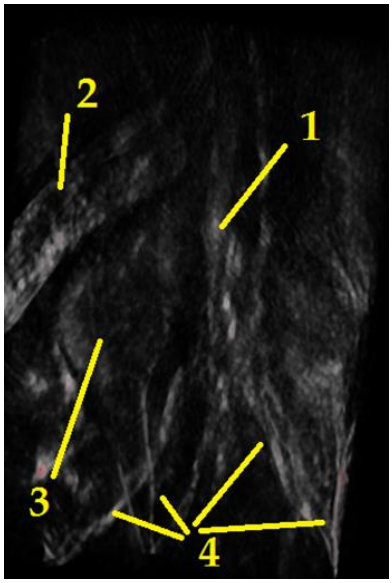

Figure 4 demonstrates some anatomical features of the mouse visible within the reconstructed PAT volume. For the used 760 nm laser excitation wavelength, deoxygenated blood dominates in optical absorption over the oxygenated blood, $\mu_a(sO_2>0.98) \approx 1/3\ \mu_a(sO_2=0)$.[31] The dorsal view of a 14 mm thick volumetric slab in the Figure 4 shows the spleen, the left kidney, the spine, the interior vena cava, and peripheral vasculature of the interrogated mouse.

Figure 4: 30 mm x 50 mm, and 14 mm thick slab of a PAT volume reconstructed from a normal mouse at 760 nm laser excitation wavelength. Dorsal view. (1) interior vena cava, (2) spleen, (3) left kidney, (4) peripheral vasculature.

In the next feasibility study, a mouse was subcutaneously administered with a 80 µL solution of indocyanine green dye (ICG) – dual fluorescent and photoacoustic contrast agent.[7] The PAFT scan was initiated immediately after the injection to observe the subcutaneous contrasted volume in both photoacoustic and fluorescent imaging modes.

For the 760 nm laser excitation wavelength, the ICG solution had a max fluorescent emission at 830 nm. The used optical emission filter (BLP01-785R-25, Semrock, Rochester, NY) had transmission T = $4.6x10^{-8}$ at 760 nm (excitation wavelength) and T = 0.98 at 830 nm (the emission max of the ICG). Transition in transmission of the emission filter extended from 800 nm (T = $1.3x10^{-4}$) to 806 nm (T = 0.65). The sCMOS camera aperture was partially open and the high gain setting was used.

Figure 5 shows multiple radial views of the studied mouse. Top set of the images was acquired by the fluorescence imaging channel. The bottom set of images – by the photoacoustic imaging channel during the same PAFT scan. The dorsal view of a 16 mm thick PAT slab shows the internal organs, systemic and peripheral blood vessels of the animal, albeit with

lower contrast than prior to the injection of ICG (Figure 4). The subcutaneous pool of ICG, injected into the rear right flank of the mouse, is well visible on both the fluorescence frames and the 3D PAT volume.

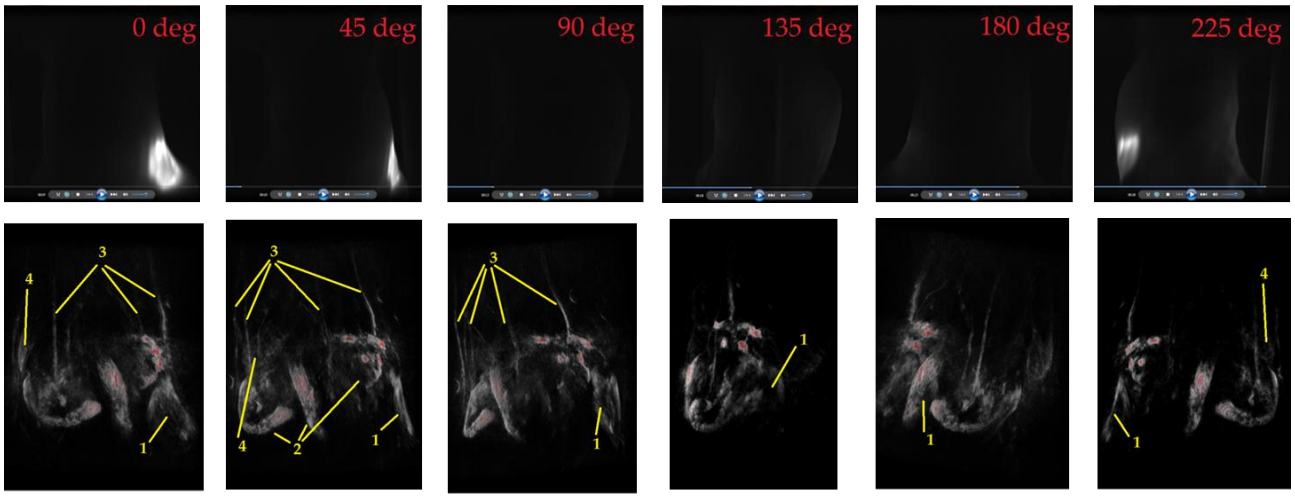

Figure 5: PAFT images of a live mouse acquired with optical excitation of 760 nm. 80 µL ICG solution was injected subcutaneously at the rear right flank of the mouse. The top set of images were acquired by the fluorescence detector. The bottom set of images were acquired by the photoacoustic detector. Azimuthal positions of the animal are indicated on the top set. At 0°, the animal is observed from the dorsal side. (1) Site of the subcutaneous ICG injection; (2) intestines; (3) blood vessels; (4) spleen.

5. CONCLUSION

In this work we demonstrated a novel tabletop 3D imaging instrument (PAFT), which combines orthogonal photoacoustic and fluorescence projections for *in vivo* preclinical imaging of murine models. The PAFT system can operate in PAT, Fluorescence or combined PAFT regimes enabling high spatial resolution and sensitivity for visualization of native chromophores (hemoglobin, oxyhemoglobin, melanin, water, and lipids), fluorophores, organic, plasmonic and carbon nanoparticles, quantum dots, and other photosensitive constructs used for *in vivo* tracking, mapping, and longitudinal studies. The 3D spatial resolution of the PAFT modality was demonstrated in phantoms to be as high as 50-100 µm, while the sensitivity in photoacoustic imaging mode enabled seeing blood vessel like targets with optical contrast of 0.6 cm^{-1}. *In vivo* imaging of a normal mouse at 760 nm laser excitation wavelength revealed central and peripheral vasculature as well as blood rich internal organs, like kidney, intestine, and spleen. It also allowed to clearly visualize a subcutaneous pool of the injected dual modality contrast agent ICG. Our ongoing efforts in the development of the introduced PAFT technology include development of a 3D fluorescence tomography algorithm, evaluation of resolution and sensitivity in the fluorescence detection mode, and further improvement of the sensitivity for photoacoustic detection.

ACKNOWLEDGMENTS

The work was supported by the grant R43OD023029 from the Office of the Director (NIH).

REFERENCES

[1] Miller, J. C., Pien, H. H., Sahani, D. *et al.*, "Imaging angiogenesis: applications and potential for drug development," J Natl Cancer Inst 97(3), 172-187 (2005).

[2] De Souza, R., Spence, T., Huang, H. *et al.*, "Preclinical imaging and translational animal models of cancer for accelerated clinical implementation of nanotechnologies and macromolecular agents," J Control Release 219, 313-330 (2015).

[3] Welsh, D. K., Kay, S. A., "Bioluminescence imaging in living organisms," Curr Opin Biotechnol 16(1), 73-78 (2005).

[4] Sutton, E. J., Henning, T. D., Pichler, B. J. *et al.*, "Cell tracking with optical imaging," Eur Radiol 18(10), 2021-2032 (2008).
[5] Ntziachristos, V., Bremer, C., Weissleder, R., "Fluorescence imaging with near-infrared light: new technological advances that enable in vivo molecular imaging," Eur Radiol 13(1), 195-208 (2003).
[6] Filonov, G. S., Piatkevich, K. D., Ting, L. M. *et al.*, "Bright and stable near-infrared fluorescent protein for in vivo imaging," Nat Biotechnol 29(8), 757-761 (2011).
[7] Fox, I. J., Wood, E. H., "Indocyanine green: physical and physiologic properties," Proc Staff Meet Mayo Clin 35, 732-744 (1960).
[8] Brecht, H. P., Su, R., Fronheiser, M. *et al.*, "Whole-body three-dimensional optoacoustic tomography system for small animals," J Biomed Opt 14(6), 064007 (2009).
[9] Ermilov, S. A., Su, R., Conjusteau, A. *et al.*, "Three-Dimensional Optoacoustic and Laser-Induced Ultrasound Tomography System for Preclinical Research in Mice: Design and Phantom Validation," Ultrason Imaging 38(1), 77-95 (2016).
[10] Xia, J., Chen, W., Maslov, K. *et al.*, "Retrospective respiration-gated whole-body photoacoustic computed tomography of mice," J Biomed Opt 19(1), 16003 (2014).
[11] Gateau, J., Caballero, M. A., Dima, A. *et al.*, "Three-dimensional optoacoustic tomography using a conventional ultrasound linear detector array: whole-body tomographic system for small animals," Med Phys 40(1), 013302 (2013).
[12] Roggan, A., Friebel, M., Doerschel, K. *et al.*, "Optical properties of circulating human blood in the wavelength range 400-2500," J Biomed Opt 4(1), 36-46 (1999).
[13] Wang, L. V., Hu, S., "Photoacoustic tomography: in vivo imaging from organelles to organs," Science 335(6075), 1458-1462 (2012).
[14] Chitnis, P. V., Brecht, H. P., Su, R. *et al.*, "Feasibility of optoacoustic visualization of high-intensity focused ultrasound-induced thermal lesions in live tissue," J Biomed Opt 15(2), 021313 (2010).
[15] Su, R., Ermilov, S. A., Liopo, A. V. *et al.*, "Three-dimensional optoacoustic imaging as a new noninvasive technique to study long-term biodistribution of optical contrast agents in small animal models," J Biomed Opt 17(10), 101506 (2012).
[16] Tsyboulski, D. A., Liopo, A. V., Su, R. *et al.*, "Enabling in vivo measurements of nanoparticle concentrations with three-dimensional optoacoustic tomography," J Biophotonics 7(8), 581-588 (2014).
[17] Stiel, A. C., Dean-Ben, X. L., Jiang, Y. *et al.*, "High-contrast imaging of reversibly switchable fluorescent proteins via temporally unmixed multispectral optoacoustic tomography," Opt Lett 40(3), 367-370 (2015).
[18] Beziere, N., Lozano, N., Nunes, A. *et al.*, "Dynamic imaging of PEGylated indocyanine green (ICG) liposomes within the tumor microenvironment using multi-spectral optoacoustic tomography (MSOT)," Biomaterials 37, 415-424 (2015).
[19] Bao, C., Beziere, N., del Pino, P. *et al.*, "Gold nanoprisms as optoacoustic signal nanoamplifiers for in vivo bioimaging of gastrointestinal cancers," Small 9(1), 68-74 (2013).
[20] Krumholz, A., Shcherbakova, D. M., Xia, J. *et al.*, "Multicontrast photoacoustic in vivo imaging using near-infrared fluorescent proteins," Sci Rep 4, 3939 (2014).
[21] Ermilov, S., Su, R., Liopo, A. *et al.*, "Optoacoustic angiography of peripheral vasculature," Proceedings of SPIE 8223, 82230D (2012).
[22] Kruger, R. A., Kuzmiak, C. M., Lam, R. B. *et al.*, "Dedicated 3D photoacoustic breast imaging," Med Phys 40(11), 113301 (2013).
[23] Razansky, D., Ntziachristos, V., "Hybrid photoacoustic fluorescence molecular tomography using finite-element-based inversion," Med Phys 34(11), 4293-4301 (2007).
[24] Kim, C., Song, K. H., Gao, F. *et al.*, "Sentinel lymph nodes and lymphatic vessels: noninvasive dual-modality in vivo mapping by using indocyanine green in rats--volumetric spectroscopic photoacoustic imaging and planar fluorescence imaging," Radiology 255(2), 442-450 (2010).
[25] Xi, L., Satpathy, M., Zhao, Q. *et al.*, "HER-2/neu targeted delivery of a nanoprobe enables dual photoacoustic and fluorescence tomography of ovarian cancer," Nanomedicine 10(3), 669-677 (2014).
[26] Wang, B., Zhao, Q., Barkey, N. M. *et al.*, "Photoacoustic tomography and fluorescence molecular tomography: a comparative study based on indocyanine green," Med Phys 39(5), 2512-2517 (2012).
[27] Deliolanis, N. C., Ale, A., Morscher, S. *et al.*, "Deep-tissue reporter-gene imaging with fluorescence and optoacoustic tomography: a performance overview," Mol Imaging Biol 16(5), 652-660 (2014).

[28] Kruger, R. A., Liu, P., Fang, Y. R. *et al.*, "Photoacoustic ultrasound (PAUS)--reconstruction tomography," Med Phys 22(10), 1605-1609 (1995).
[29] Xu, M. H., Wang, L. H. V., "Time-domain reconstruction for thermoacoustic tomography in a spherical geometry," Ieee Transactions on Medical Imaging 21(7), 814-822 (2002).
[30] Finch, D., Patch, S. K., Rakesh, "Determining a function from its mean values over a family of spheres," SIAM J. Math. Anal. 35(5), 1213-1240 (2004).
[31] Bosschaart, N., Edelman, G. J., Aalders, M. C. *et al.*, "A literature review and novel theoretical approach on the optical properties of whole blood," Lasers Med Sci 29(2), 453-479 (2014).